

Article

Synthesis and Properties of Nanosized Stoichiometric Cobalt Ferrite Spinel

Vilém Bartůněk¹, David Sedmidubský¹ , Štěpán Huber¹, Marie Švecová^{2,3}, Pavel Ulbrich⁴ and Ondřej Jankovský^{1,*}

¹ Department of Inorganic Chemistry, Faculty of Chemical Technology, University of Chemistry and Technology, Technická 5, 166 28 Prague 6, Czech Republic; Vilem.Bartunek@vscht.cz (V.B.); David.Sedmidubsky@vscht.cz (D.S.); Stepan.Huber@vscht.cz (Š.H.)

² Department of Analytical Chemistry, Faculty of Chemical Engineering, University of Chemistry and Technology, Technická 5, 166 28 Prague 6, Czech Republic; Marie.Svecova@vscht.cz

³ Department of Physical Chemistry, Faculty of Chemical Engineering, University of Chemistry and Technology, Technická 5, 166 28 Prague 6, Czech Republic

⁴ Department of Biochemistry and Microbiology, Faculty of Food and Biochemical Technology, University of Chemistry and Technology, Technická 5, 166 28 Prague 6, Czech Republic; Pavel.Ulbrich@vscht.cz

* Correspondence: Ondrej.Jankovsky@vscht.cz; Tel.: +420-220-44-2002

Received: 23 June 2018; Accepted: 16 July 2018; Published: 19 July 2018



Abstract: Nanoparticles with controllable sizes of ferrite spinel CoFe_2O_4 were formed by thermal treatment of cobalt-iron glycerolate. Thermal behavior during the heating was studied by differential thermal analysis combined with thermogravimetry. The precursor, as well as the prepared nanoparticles, were analyzed by a broad spectrum of analytic techniques (X-Ray photoelectron spectroscopy (XPS), X-Ray diffraction (XRD), Energy dispersive spectroscopy (EDS), Atomic absorption spectroscopy (AAS), Scanning electron microscopy (SEM), and Raman spectroscopy). The particle size of nanoparticles was obtained from Transmission electron microscopy and also calculated using Scherrer formula. A vibrating sample magnetometer (VSM) in a Physical Property Measurement System was used to analyze the magnetic properties of nanoparticles.

Keywords: nanoparticles; ferrites; thermal decomposition; spinels; magnetic properties

1. Introduction

As a part of the ferrite family, magnetic CoFe_2O_4 spinel is in the focus of research because of its potential use in various applications. Due to its magnetic properties, CoFe_2O_4 nanoparticles may be employed in catalysts [1,2], cathode electrocatalyst of microbial fuel cells [3], or in various functional composite materials [4,5], including advanced adsorbents, for the removal of anionic pollutants from water [6]. Cobalt ferrite has been also considered as a good candidate for biomedical applications [7–9], especially for hyperthermia treatment, because of its high magneto-crystalline anisotropy [7].

Nanosized ferrites may be synthesized in many ways. A usual synthetic technique for preparation of magnetic CoFe_2O_4 nanoparticles is the co-precipitation method [1–13], but also hydrothermal [14–17], sol-gel auto-combustion [18,19], and microwave assisted [20,21] methods can be applied.

Thermal treatment of glycerol-based organometallic compounds (glycerolates) can be used for synthesis of nanoparticles with variable sizes, e.g., cobalt oxides [22], iron oxide [23], manganese oxides [24,25], and chromium oxide [26]. In addition, mixed ferrites, such as NiFe_2O_4 [27], have been synthesized and, through the use of a reduction atmosphere, some pure metallic nanoobjects, e.g., cobalt nanofoam [28], can be prepared. As a solvent, template compound or chelation agent, e.g., glycerol,

is particularly advantageous. It exhibits a high boiling point and its viscosity is notably dependent on temperature and water dilution, therefore it is easily controllable for the purpose of nanoparticle stabilization. Furthermore, it is extra affordable in comparison with similar compounds and accessible in large quantities—therefore, the methods relying on glycerol-based precursors may have a good outlook for large-scale industrial application.

In our contribution, we focused on the synthesis of CoFe_2O_4 nanoparticles. Cobalt-iron glycerolate and CoFe_2O_4 nanoparticles were analyzed in detail by a broad spectrum of analytic techniques. The main focus was given to magnetic properties of CoFe_2O_4 spinel.

2. Materials and Methods

Cobalt-iron glycerolate was synthesized by a reaction of glycerol (in excess) with $\text{Fe}(\text{NO}_3)_3$ and $\text{Co}(\text{NO}_3)_2$ mixed in the target molar proportion 2:1. The synthesis was performed under reflux of glycerol (boiling, 290 °C) for four hours without using any additional atmosphere. After the heat treatment, the mixture was put into water and the solid phase was subsequently obtained by centrifugation. The obtained solid material was washed using distilled water and ethanol and dried. The prepared glycerolate was labeled as Co-Fe-GLY. The synthesized cobalt-iron glycerolate was thermally decomposed in the tube furnace in a dynamic air atmosphere ($p_{\text{O}_2}/p^0 = 0.21$, $p^0 = 101$ kPa). The temperatures applied were the following: 500 °C, 600 °C, 700 °C, or 800 °C for 1 minute (rates 10 K min^{-1}). The prepared nanoparticles were termed as Co-Fe-500, Co-Fe-600, Co-Fe-700, and Co-Fe-800, accordingly.

X-Ray diffraction (XRD) patterns were measured using Bruker D2 Phaser (Bruker, Karlsruhe, Germany) powder diffractometer (Bragg-Brentano geometry) using $\text{CoK}\alpha$ radiation ($\lambda = 0.1789$ Å, $U = 40$ kV, $I = 30$ mA).

X-Ray photoelectron spectroscopy (XPS) was measured with ESCAProbeP (Omicron Nanotechnology Ltd, East Grinstead, UK) spectrometer using a monochromatic aluminum X-ray radiation source (1486.7 eV).

Scanning electron microscopy (SEM) with a FEG electron source (Lyra, Tescan, Brno, Czech Republic) was used to investigate the morphology. Elemental composition was performed using an Energy dispersive spectroscopy (EDS) analyzer (X-Max^N) with a 20 mm² SDD (Silicon Drift Detector) (X-Max^N, Oxford instruments, Abingdon-on-Thames, UK) and AZtecEnergy software (v 2.1, Oxford instruments, Abingdon-on-Thames, UK). Measurements were carried out using 10 kV electron beam.

Atomic absorption spectroscopy (AAS) was used to determine the concentration of metal elements using Agilent 280FS AA device (Agilent Technologies, Mulgrave, Australia) with a flame-atomization technique. The used wavelengths were 240.7 nm for cobalt and 248.3 nm for iron. Acetylene-air flame was used for the measurement.

Raman spectroscopy was measured using confocal Raman microspectrometer Renishaw inVia Reflex (Renishaw, Wotton under Edge, UK) equipped with a diode laser (excitation line 785 nm).

The thermal behavior was probed by simultaneous thermal analysis (STA) using Linseis STA PT1600 apparatus (Linseis Messgeraete GmbH, Selb, Germany) with the heating rate 10 K min^{-1} in dynamic air atmosphere.

Transmission electron microscopy (TEM) was performed using microscope JEOL JEM-1010 (JEOL, Tokyo, Japan) at an accelerating voltage of 80 kV. The micrographs were acquired by SIS MegaView III digital camera (Soft Imaging Systems, Münster, Germany) and analyzed by means of AnalySIS v. 2.0 software.

Vibrating sample magnetometer (VSM) installed in Physical Property Measurement System (PPMS, Quantum Design, San Diego, CA, USA) was used for the measurements of the magnetization curves ($\mu_0 H = +7$ to -7 T, $T = 4.5$ and 300 K) and for the magnetic susceptibility in the temperature range 4.5–340 K (applied magnetic field $\mu_0 H = 0.1$ T). The field cooled (FC) susceptibility was acquired on cooling in the magnetic field in a sweeping mode (cooling rate 5 K min^{-1}), while the zero-field cooled (ZFC) susceptibility was measured on heating (heating rate 5 K min^{-1}) after cooling the sample in zero field and then switching on the field. The vibrating frequency was 60 Hz and the amplitude 1 mm.

3. Results and Discussion

The successful synthesis of cobalt-iron glycerolate (Ni-Fe-GLY) was confirmed by XRD. The observed XRD pattern is shown in Figure 1. Similar to manganese glycerolate [24], a wide reflection (at $2\theta = 12.78$) was observed, confirming that the synthesized glycerolate was highly non-crystalline or nanostructured.

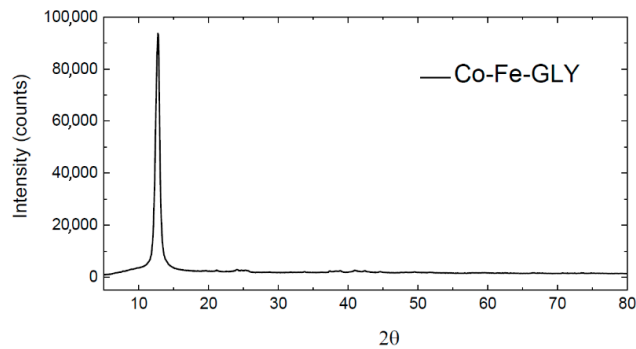


Figure 1. Diffractogram of Co-Fe-GLY.

Cobalt-iron glycerolate was studied using SEM and EDS. Large agglomerates with a size over 20 μm were found; only few particles were of sub-micron size (see Figure 2). Let us note that a similar structure has been also obtained for other glycerolates [22–24]. SEM-EDS spectrum is shown in Figure 3, confirming the presence of carbon, oxygen, iron, and cobalt. Gold, originating from the sputtering, was also detected. The obtained composition $\text{Co}_1\text{Fe}_{2.02}\text{C}_{10.7}\text{O}_{7.76}$ (Co stoichiometry was fixed to 1) was determined as an average from four measurements. The corresponding C/O ratio was $\sim 1.38:1$, which was further confirmed by AAS. Similarly, the ratio of metals in cobalt-iron glycerolate 1:2.08 as obtained from AAS is in line with SEM-EDS results.

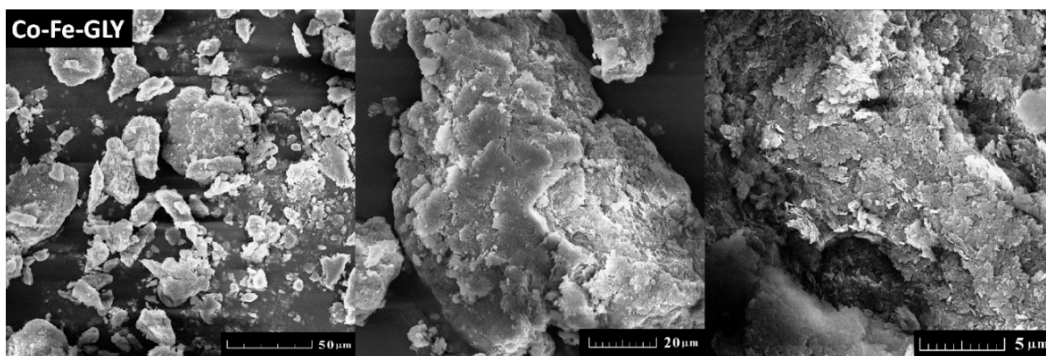


Figure 2. SEM micrographs of Co-Fe-GLY obtained at various magnifications.

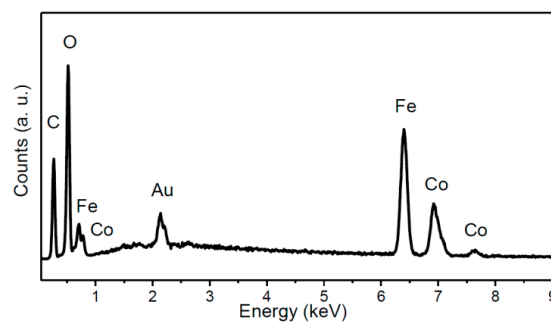


Figure 3. EDS spectrum of Co-Fe-GLY.

The Co-Fe-GLY composition was examined by XPS (Figure 4). The Co2p, Fe2p, C1s, and O1s peaks were identified in the obtained survey spectrum. The first peak corresponding to C1s was obtained at ~286.5 eV. A peak corresponding to O1s was found at ~531.6 eV. A third peak observed at ~712.5 eV can be attributed to Fe2p. The last peak was found at ~782.4 eV, this Co2p peak confirmed the presence of cobalt in the glycerolate. The observed positions for Co2p and Fe2p are in good agreement with the literature [29]. Chemical composition $\text{Co}_1\text{Fe}_{1.80}\text{C}_{42.06}\text{O}_{25.57}$ (Co being fixed to 1) was calculated from the spectrum. The C/O ratio ~1.64:1 was slightly higher to that determined by SEM-EDS. The composition of bulk cobalt-iron glycerolate probed by XPS is slightly different compared to EDS results due to a surface sensitivity of XPS.

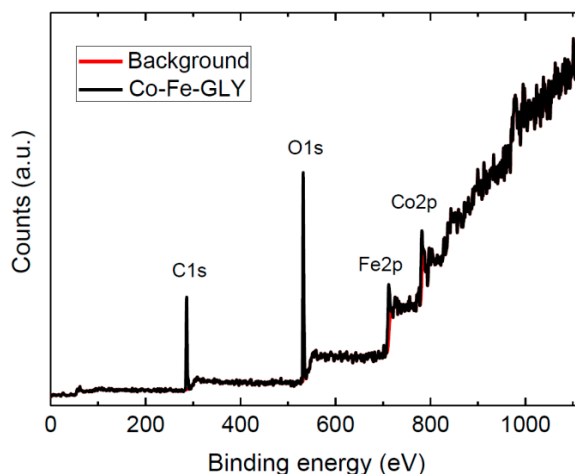


Figure 4. XPS survey spectrum of Co-Fe-GLY.

Thermal behavior was studied by thermal analysis. As seen from Figure 5, one exothermic effect was observed; however, this effect is clearly composed of three partial transitions. The first exo-peak started at ~150 °C and reached its maximum at 185 °C, the second major exo-effect reached the maximum at 298 °C, while the third one was indicated at 399 °C. The thermal decomposition led to a formation of pure nanoparticles, which will be discussed later. The decomposition/oxidation was accompanied by a weight loss of ~45 wt. %. Assuming the formation of pure CoFe_2O_4 , we can estimate the glycerolate molar mass as 425.6 g mol^{-1} , corresponding well with the chemical composition determined by EDS.

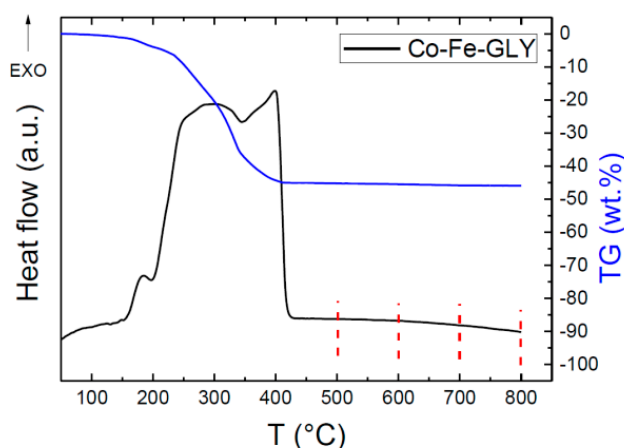


Figure 5. STA analysis of Co-Fe-GLY with marked decomposition temperatures.

Based on the XRD analysis, it can be confirmed that nanocrystalline CoFe_2O_4 was obtained (Figure 6) [30]. Next, Scherrer formula was used to determine the crystallite sizes. The results confirmed the expected behavior: At higher temperatures, nanocrystal growth took place, hence bigger nanoparticles were formed. The calculated crystallite sizes of CoFe_2O_4 were ~ 6.2 nm, ~ 9.7 nm, ~ 17.5 nm, and ~ 28.2 nm for the samples Co-Fe-500, Co-Fe-600, Co-Fe-700, and Co-Fe-800, respectively. The evolution of particle size with temperature is obvious. The acquired diffraction patterns are in good agreement to the literature [29,31].

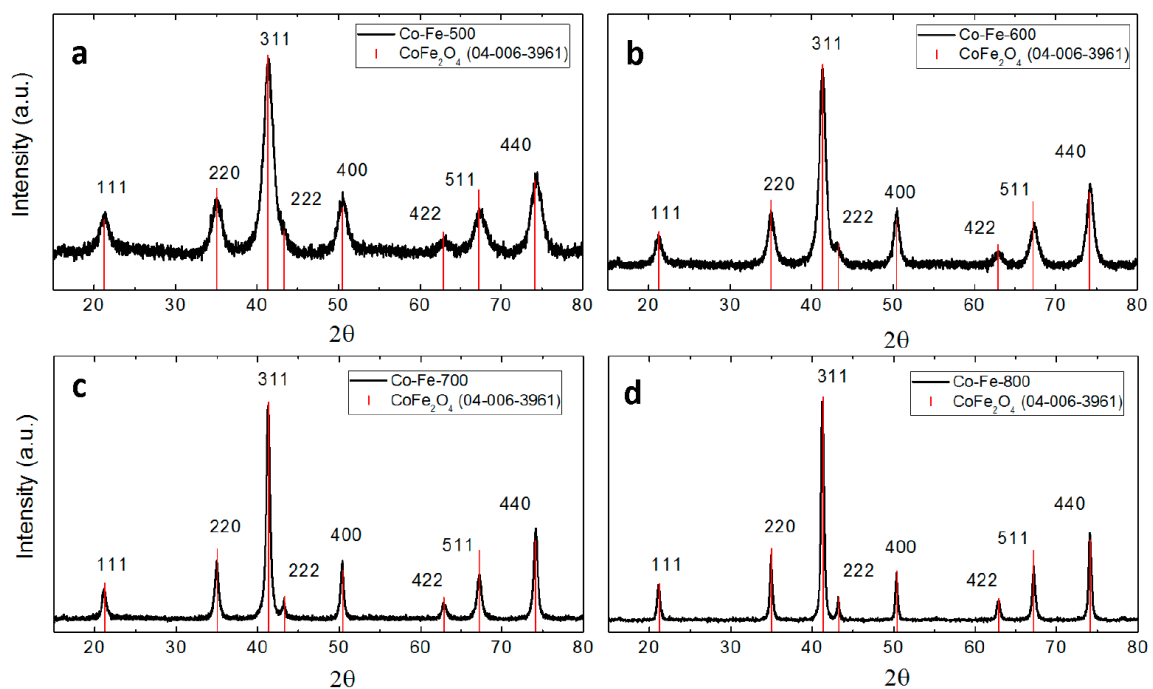


Figure 6. XRD patterns of prepared nanoparticles: (a) Co-Fe-500, (b) Co-Fe-600, (c) Co-Fe-700 and (d) Co-Fe-800.

Transmission electron microscopy (TEM) was applied in order to prove the calculated particle diameters (Figure 7). While the nanoparticles Co-Fe-500 and Co-Fe-600 are ultrafine with homogenous particle size distribution, the other two samples prepared at higher temperatures significantly differed due to crystallite growth resulting in larger nanoparticles with different shapes and divergent particle sizes. However, it was proved that particle diameters are growing with increasing temperature. The histograms showing the particle size distribution of the selected area are also shown in Figure 7.

The Raman spectroscopy confirmed the presence of an inverse spinel structure $\text{Fe}[\text{CoFe}]\text{O}_4$ [32–34], without any indication of signals belonging to impurity phases, such as those corresponding to precursors. The Raman spectra are shown in Figure 8. The bands at 1325 and 1135 cm^{-1} are assigned to the A_{1g} and T_{2g} modes of the 2nd order. The next bands at 692 cm^{-1} and at 615 cm^{-1} correspond to A_{1g} symmetric stretching (tetrahedral breath mode) of oxygen atoms with respect to Fe and Co ions. T_{2g} modes (asymmetric stretching and bending, respectively) are assigned to bands at the 553 and 473 cm^{-1} , and the T_{2g} mode at 183 cm^{-1} belongs to a translation motion of the whole tetrahedron. The band at 297 cm^{-1} is assigned to E_g symmetric bending of Fe(Co)-O. The results of Raman analysis are also summarized in Table 1.

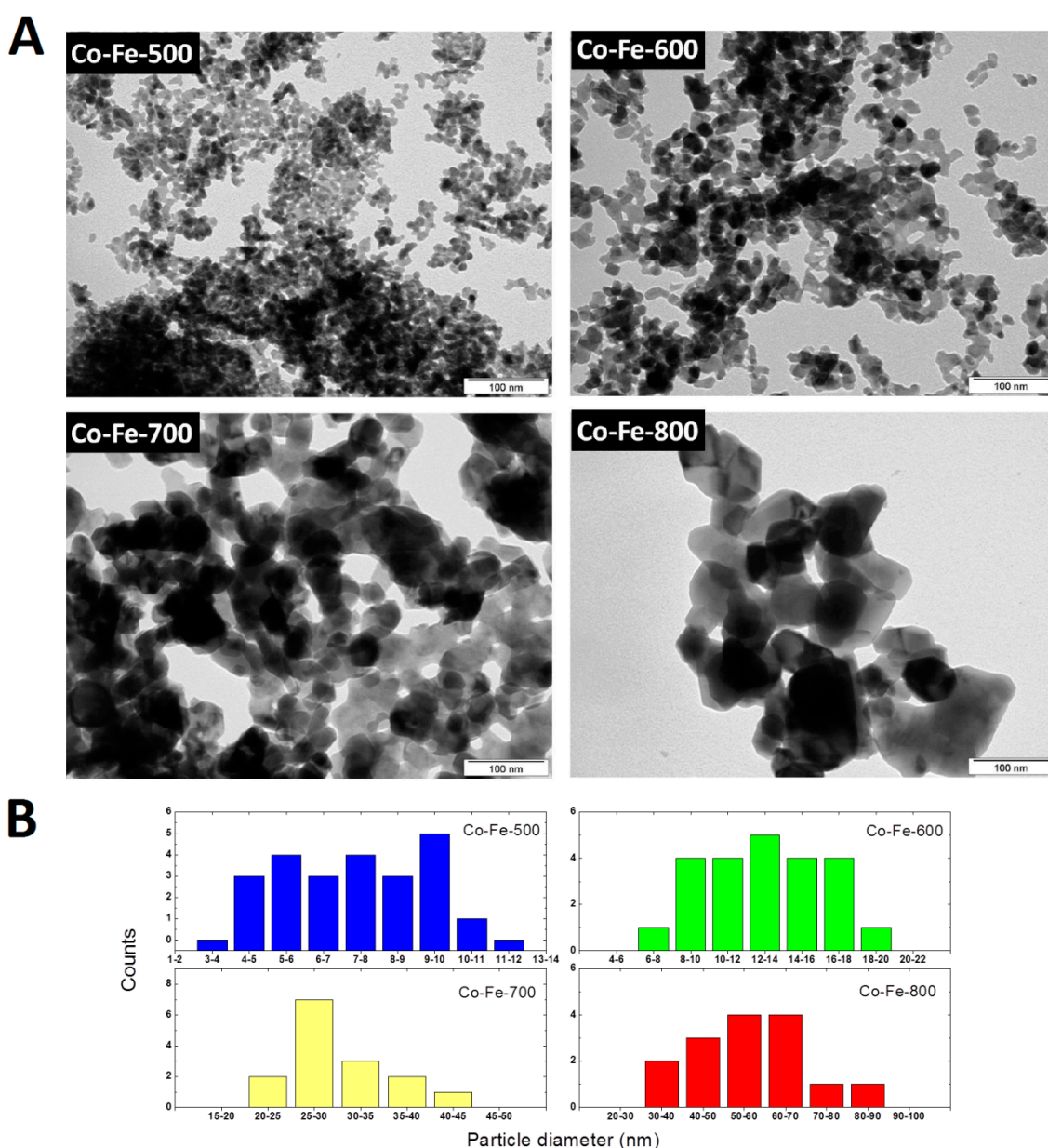


Figure 7. (A) TEM micrographs of synthesized nanoparticles; (B) particle size distribution obtained by image analysis.

CoFe_2O_4 in a bulk form is known to exist predominantly in the inverse spinel structure (with only 10–20 per cent of Co occupying the tetrahedral sites). Considering of a 90° superexchange interaction between both types of cations occupying the octahedral sites ($\text{Co}^{2+}-3d^7$ and $\text{Fe}^{3+}-3d^5$, both occurring in high spin state) leading to parallel spin ordering, and an antiferromagnetic coupling between the tetrahedral (spin $S = 5/2$) and octahedral positions ($S = 4$), we can anticipate a ferrimagnetic behavior with a saturated magnetic moment $M_{\text{sat}} \sim 3 \mu_{\text{B}}$ ($S = 3/2$) per formula unit (f.u.). Such behavior is indeed observed below the Curie temperature $T_{\text{C}} \sim 793$ K. These experimental findings are in line with our DFT calculations (GGA+U, APW+lo, as implemented in Wien2k), confirming the inverse spinel structure (favored by 50 kJ mol^{-1} with respect to normal spinel) and the AF interaction between the tetrahedral Fe^{3+} and mixed $\text{Co}^{2+}/\text{Fe}^{3+}$ octahedral sites. The integrated density of states for spin-up and spin-down channel, as shown in Figure 9, yields the net magnetic moment $3 \mu_{\text{B}}$.

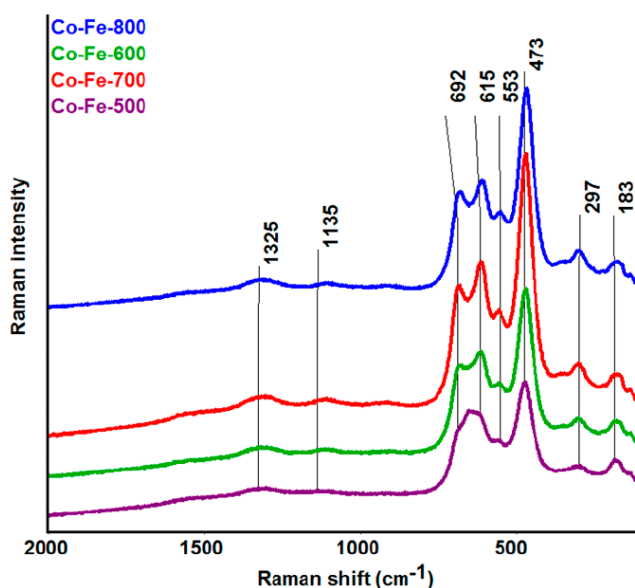


Figure 8. Raman spectra of CoFe₂O₄ nanoparticles prepared at various temperatures.

Table 1. Measured Raman shifts of CoFe₂O₄ nanoparticles.

Experimental	Raman Shift (cm ⁻¹)		Vibrational Mode	Assignment
	Wang et al. [32]	Chandramohan et al. [33]		
1325	-	-	A _{1g}	2nd order bands
1135	-	-	T _{2g} (2)	
692	683	695	A _{1g} (1)	symmetric stretching Fe-O
615	617	624	A _{1g} (2)	symmetric stretching Fe(Co)-O
553	563	575	T _{2g} (2)	asymmetric stretching Fe-O
473	471	470	T _{2g} (3)	asymmetric bending Fe(Co)-O
297	300	312	E _g	symmetric bending Fe(Co)-O
183	188	210	T _{2g} (1)	translation motion of the whole tetrahedron

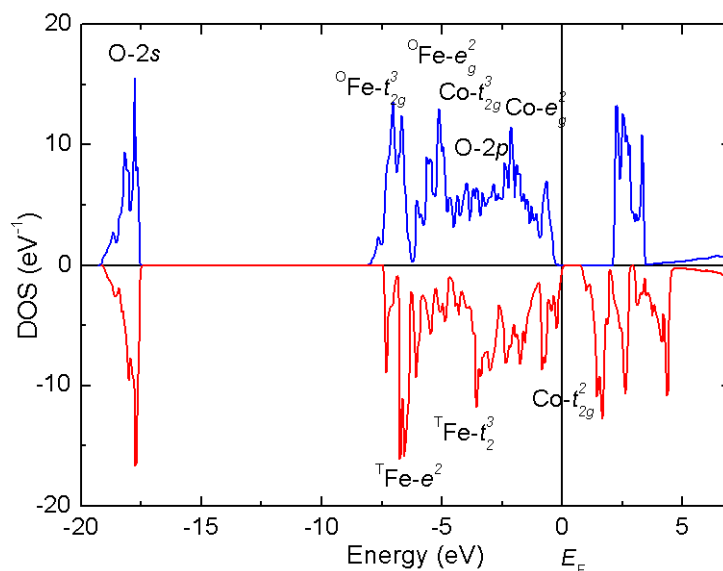


Figure 9. Density of states (DOS) around the Fermi level E_F of the inverse spinel structure, Fe³⁺[Fe³⁺Co²⁺]O₄. The majority spin (blue, positive): Co, Fe(oct)- $t_{2g}^3e_g^2$. Minority spin (red, negative): Fe(tet)- $e^2t_2^3$, Co(oct)- t_{2g}^2 .

The magnetization curves measured at $T = 300$ K and at $T = 4.5$ K (Figure 10) reveal a saturation, though not complete, at higher magnetic fields, which is substantially suppressed compared to the bulk form and decreases with reducing crystallite size. The main parameters of the obtained magnetization curves are summarized in Table 2.

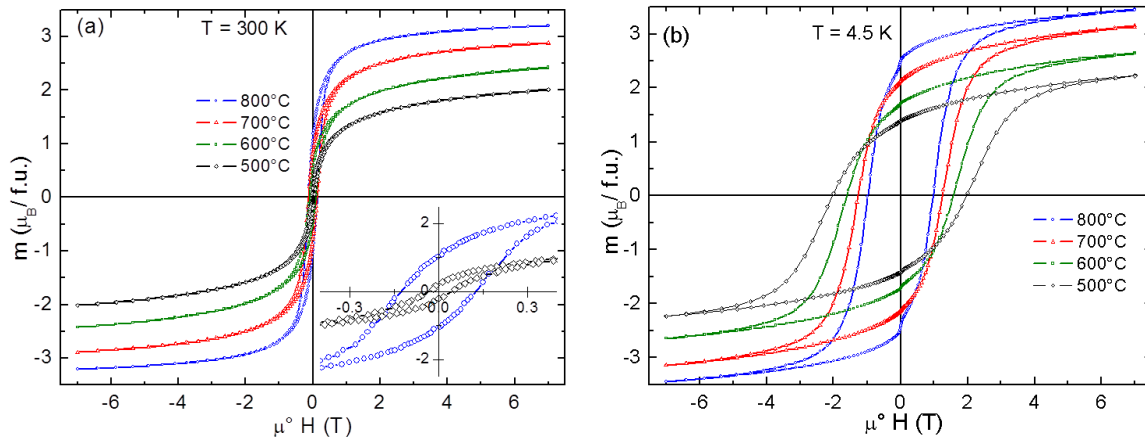


Figure 10. Magnetization curves of CoFe_2O_4 recorded at 300 K (a) and 4.5 K (b). A blow-up of two hysteresis curves (Co-Fe-500 and Co-Fe-800) is shown in the inset of panel (a).

Table 2. Coercivity field $\mu^{\circ}H_c$, remanent magnetization M_r , magnetic moment at the maximum field M_{7T} obtained from the magnetization curves measured at 300 K and 4.5 K, and the blocking temperature T_B determined as a furcation point between field cooled and zero-field cooled (FC and ZFC) curves of magnetic susceptibility.

Co-Fe	$\mu^{\circ}H_c$ (300 K) mT	M_r (300 K) $\mu_B/\text{f.u.}$	M_{7T} (300 K) $\mu_B/\text{f.u.}$	$\mu^{\circ}H_c$ (4.5 K) T	M_r (4.5 K) $\mu_B/\text{f.u.}$	M_{7T} (4.5 K) $\mu_B/\text{f.u.}$	T_B K
500	45	0.20	2.00	1.95	1.36	2.23	340
600	90	0.51	2.41	1.58	1.72	2.65	328
700	138	0.81	2.89	1.28	2.13	3.15	300
800	130	1.20	3.20	0.99	2.47	3.46	300

Only a small hysteresis is observed on the magnetization curves recorded at $T = 300$ K (coercivity field ranging from $\mu^{\circ}H_c = 45$ mT to $\mu^{\circ}H_c = 130$ mT for Co-Fe-500 and Co-Fe-800, respectively). This behavior, together with a notable difference between the zero-field cooled (ZFC) and field cooled (FC) magnetic susceptibility below room temperature (see Figure 11), suggests a superparamagnetic (SPM) behavior. Superparamagnetic behavior of nanoparticles (5–8 nm) at room temperature was already identified by Repko et al. [35].

Interestingly, the FC susceptibility of Co-Fe-500 sample undergoes an upturn from the slightly decreasing trend at 300 K before merging the ZFC curve at the blocking temperature $T_B \sim 340$ K. (determined as a furcation point of the ZFC-FC curves). Blocking temperatures in the range 200–400 K have been reported for various CoFe_2O_4 nanoparticles [35].

At lower temperatures, the slow relaxation brings about a pronounced hysteresis, which increases with reducing particle size and reaches the highest coercivity field $\mu^{\circ}H_c = 2$ T for Co-Fe-500 and the highest remanence $M_r \sim 2.5 \mu_B/\text{f.u.}$ for Co-Fe-800. Let us note that much smaller hysteresis ($\mu^{\circ}H_c = \sim 120$ mT) and also a lower blocking temperatures T_B have been recently found in NiFe_2O_4 inverse spinels [27] with comparable particle sizes. This can be in part interpreted in terms of larger magnetic anisotropy of CoFe_2O_4 ($K_1 = 2 \times 10^6$ as compared with $K_1 = -5 \times 10^4$ for NiFe_2O_4 [36]), bringing about a higher blocking temperature, however, magnetic frustration due to competing exchange interactions, as well as site and displacive disorder associated with the surface states, might be at the origin of this huge hysteresis.

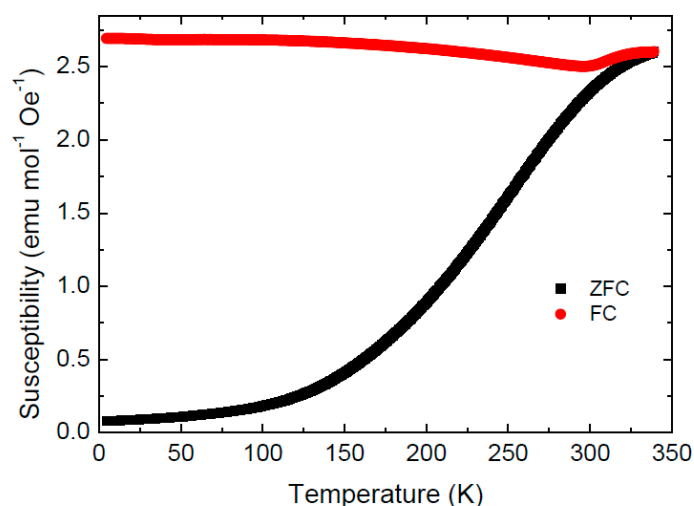


Figure 11. Field cooled (FC) and zero field cooled (ZFC) magnetic susceptibility of Co-Fe-500 sample measured in the temperature sweeping mode at a heating and cooling rate 5 K min^{-1} .

The observed magnetic behavior makes cobalt ferrite nanoparticles excellent candidates for hyperthermia treatment and other medicinal applications. The particle size control, as demonstrated on the proposed thermal decomposition of glycerolates, is indeed essential for tailoring the nanomaterial magnetic properties

One of the main advantages of the described synthesis method of CoFe_2O_4 nanoparticles in comparison with co-precipitation or hydrothermal methods is the absence of other elements and ions, e.g., Na^+ ions in the case of co-precipitation methods or various capping agents in the case of usual hydrothermal techniques. The ability to control the nanoparticles size also represents a great advantage of the present method. Moreover, the method operates with affordable, non-toxic and available precursors, and is usable even for preparation of larger amounts of the material, therefore with the possibility for further development for applications on an industrial scale.

4. Conclusions

Cobalt ferrite spinel nanoparticles with stoichiometry CoFe_2O_4 were synthesized by thermal decomposition of cobalt-iron glycerolate. Nanoparticles' sizes were controlled by temperature of decomposition of previously synthesized glycerolate precursor in the range from 6.2 to 28.2 nm. Both precursor and product were characterized by various means, including Raman spectroscopy, XRD, SEM-EDS, TEM, AAS, and XPS. The CoFe_2O_4 spinel nanoparticles exhibit a pronounced hysteresis, a suppressed saturated magnetization, and high blocking temperatures due to large magnetic anisotropy and nanosizing effects. Our method may be applied for preparation of high volumes of magnetic CoFe_2O_4 nanoobjects of selected sizes with a surface free of surfactant or other contamination.

Author Contributions: V.B., O.J. and D.S. wrote the manuscript. V.B. and O.J. prepared samples. V.B., D.S., Š.H., M.Š., P.U. and O.J. analyzed the samples. **Funding:** This work was supported by Czech Science Foundation, grant no. 17-13161S and by Ministry of Education of the Czech Republic, grant number 20/2018 for specific university research.

Conflicts of Interest: The authors declare no conflict of interest, the funders had no role in the design of the study; in the collection, analyses, or interpretation of data; in the writing of the manuscript, and in the decision to publish the results.

References

1. He, S.H.; Shi, W.B.; Zhang, X.D.; Li, J.A.; Huang, Y.M. Beta-cyclodextrins-based inclusion complexes of CoFe_2O_4 magnetic nanoparticles as catalyst for the luminol chemiluminescence system and their applications in hydrogen peroxide detection. *Talanta* **2010**, *82*, 377–383. [[CrossRef](#)] [[PubMed](#)]
2. Rajput, J.K.; Kaur, G. Synthesis and applications of CoFe_2O_4 nanoparticles for multicomponent reactions. *Catal. Sci. Technol.* **2014**, *4*, 142–151. [[CrossRef](#)]
3. Huang, Q.S.; Zhou, P.J.; Yang, H.; Zhu, L.L.; Wu, H.Y. In situ generation of inverse spinel CoFe_2O_4 nanoparticles onto nitrogen-doped activated carbon for an effective cathode electrocatalyst of microbial fuel cells. *Chem. Eng. J.* **2017**, *325*, 466–473. [[CrossRef](#)]
4. Mordina, B.; Tiwari, R.K.; Setua, D.K.; Sharma, A. Superior elastomeric nanocomposites with electrospun nanofibers and nanoparticles of CoFe_2O_4 for magnetorheological applications. *RSC Adv.* **2015**, *5*, 19091–19105. [[CrossRef](#)]
5. Saffari, J.; Ghanbari, D.; Mir, N.; Khandan-Barani, K. Sonochemical synthesis of CoFe_2O_4 nanoparticles and their application in magnetic polystyrene nanocomposites. *J. Ind. Eng. Chem.* **2014**, *20*, 4119–4123. [[CrossRef](#)]
6. Santhosh, C.; Daneshvar, E.; Kollu, P.; Peraniemi, S.; Grace, A.N.; Bhatnagar, A. Magnetic $\text{SiO}_2\text{-CoFe}_2\text{O}_4$ nanoparticles decorated on graphene oxide as efficient adsorbents for the removal of anionic pollutants from water. *Chem. Eng. J.* **2017**, *322*, 472–487. [[CrossRef](#)]
7. Lima-Tenorio, M.K.; Tenorio-Neto, E.T.; Hechenleitner, A.A.W.; Fessi, H.; Pineda, E.A.G. CoFe_2O_4 and ZnFe_2O_4 nanoparticles: An overview about structure, properties, synthesis and biomedical applications. *J. Colloid Sci. Biotechnol.* **2016**, *5*, 45–54. [[CrossRef](#)]
8. Momin, N.; Deshmukh, A.; Radha, S. Synthesis and characterization of $\text{CoFe}_2\text{O}_4\text{-NiFe}_2\text{O}_4$ magnetic nanoparticles for various biomedical applications: cell viability and cell death evaluations. *J. Nano Res.* **2015**, *34*, 1–8. [[CrossRef](#)]
9. Munjal, S.; Khare, N.; Nehate, C.; Koul, V. Water dispersible CoFe_2O_4 nanoparticles with improved colloidal stability for biomedical applications. *J. Magn. Magn. Mater.* **2016**, *404*, 166–169. [[CrossRef](#)]
10. Prabhakaran, T.; Mangalaraja, R.V.; Denardin, J.C.; Jimenez, J.A. The effect of calcination temperature on the structural and magnetic properties of co-precipitated CoFe_2O_4 nanoparticles. *J. Alloys Compd.* **2017**, *716*, 171–183. [[CrossRef](#)]
11. Kumar, A.; Yadav, N.; Rana, D.S.; Kumar, P.; Arora, M.; Pant, R.P. Structural and magnetic studies of the nickel doped CoFe_2O_4 ferrite nanoparticles synthesized by the chemical co-precipitation method. *J. Magn. Magn. Mater.* **2015**, *394*, 379–384. [[CrossRef](#)]
12. Safi, R.; Ghasemi, A.; Shoja-Razavi, R. Factors controlling magnetic properties of CoFe_2O_4 nanoparticles synthesized by chemical co-precipitation: Modeling and optimization using response surface methodology. *Ceram. Int.* **2016**, *42*, 15818–15825. [[CrossRef](#)]
13. Safi, R.; Ghasemi, A.; Shoja-Razavi, R.; Ghasemi, E.; Sodaee, T. Rietveld structure refinement, cations distribution and magnetic features of CoFe_2O_4 nanoparticles synthesized by co-precipitation, hydrothermal, and combustion methods. *Ceram. Int.* **2016**, *42*, 6375–6382. [[CrossRef](#)]
14. Jalalian, M.; Mirkazemi, S.M.; Alamolhoda, S. Phase constituents and magnetic properties of the CoFe_2O_4 nanoparticles prepared by polyvinylpyrrolidone (PVP)-assisted hydrothermal route. *Appl. Phys. A* **2016**, *122*, 835. [[CrossRef](#)]
15. Liu, M.; Lu, M.; Wang, L.; Xu, S.C.; Zhao, J.L.; Li, H.B. Mossbauer study on the magnetic properties and cation distribution of CoFe_2O_4 nanoparticles synthesized by hydrothermal method. *J. Mater. Sci.* **2016**, *51*, 5487–5492. [[CrossRef](#)]
16. Rafique, M.Y.; Pan, L.Q.; Javed, Q.U.A.; Iqbal, M.Z.; Yang, L.H. Influence of NaBH_4 on the size, composition, and magnetic properties of CoFe_2O_4 nanoparticles synthesized by hydrothermal method. *J. Nanopart. Res.* **2012**, *14*, 1189. [[CrossRef](#)]
17. Suwanchawalit, C.; Somjit, V. A facile hydrothermal synthesis of magnetic CoFe_2O_4 nanoparticles and photocatalytic performance. *Dig. J. Nanomater. Biostruct.* **2015**, *10*, 705–713.
18. Yadav, R.S.; Havlica, J.; Masilko, J.; Kalina, L.; Hajduchova, M.; Enev, V.; Wasserbauer, J.; Kuritka, I.; Kozakova, Z. Structural, cation distribution, and magnetic properties of CoFe_2O_4 spinel ferrite nanoparticles synthesized using a starch-assisted sol-gel auto-combustion method. *J. Supercond. Nov. Magn.* **2015**, *28*, 1851–1861. [[CrossRef](#)]

19. Yadav, R.S.; Havlica, J.; Ptacek, P.; Kuritka, I.; Kozakova, Z.; Palou, M.; Bartonickova, E.; Bohac, M.; Frajkorova, F.; Masilko, J.; et al. Structural and magnetic properties of CoFe_2O_4 nanoparticles synthesized by starch-assisted sol-gel auto-combustion method in air, argon, nitrogen and vacuum atmospheres. *J. Supercond. Nov. Magn.* **2015**, *28*, 249–258. [[CrossRef](#)]
20. Amiri, G.R.; Yousefi, M.H.; Fatahian, S. Magnetic properties of CoFe_2O_4 and $\text{Co}_{0.5}\text{Zn}_{0.5}\text{Fe}_2\text{O}_4$ ferrite nanoparticles synthesized by microwave method. *Optoelectron. Adv. Mater.-Rapid Commun.* **2012**, *6*, 158–161.
21. Bartolome, E.; Cayado, P.; Solana, E.; Ricart, S.; Gazquez, J.; Mundet, B.; Coll, M.; Puig, T.; Obradors, X.; Valvidares, M.; et al. Magnetic stability against calcining of microwave-synthesized CoFe_2O_4 nanoparticles. *New J. Chem.* **2016**, *40*, 6890–6898. [[CrossRef](#)]
22. Bartunek, V.; Huber, S.; Sedmidubsky, D.; Sofer, Z.; Simek, P.; Jankovsky, O. CoO and Co_3O_4 nanoparticles with a tunable particle size. *Ceram. Int.* **2014**, *40*, 12591–12595. [[CrossRef](#)]
23. Bartunek, V.; Prucha, D.; Svecova, M.; Ulbrich, P.; Huber, S.; Sedmidubsky, D.; Jankovsky, O. Ultrafine ferromagnetic iron oxide nanoparticles: Facile synthesis by low temperature decomposition of iron glycerolate. *Mater. Chem. Phys.* **2016**, *180*, 272–278. [[CrossRef](#)]
24. Jankovsky, O.; Sedmidubsky, D.; Simek, P.; Sofer, Z.; Ulbrich, P.; Bartunek, V. Synthesis of MnO , Mn_2O_3 and Mn_3O_4 nanocrystal clusters by thermal decomposition of manganese glycerolate. *Ceram. Int.* **2015**, *41*, 595–601. [[CrossRef](#)]
25. Pinc, J.; Jankovský, O.; Bartůněk, V. Preparation of manganese oxide nanoparticles by thermal decomposition of nanostructured manganese carbonate. *Chem. Pap.* **2017**, *71*, 1031–1035. [[CrossRef](#)]
26. Jankovsky, O.; Sedmidubsky, D.; Sofer, Z.; Luxa, J.; Bartunek, V. Simple synthesis of Cr_2O_3 nanoparticles with a tunable particle size. *Ceram. Int.* **2015**, *41*, 4644–4650. [[CrossRef](#)]
27. Jankovský, O.; Rach, V.; Sedmidubský, D.; Huber, Š.; Ulbrich, P.; Švecová, M.; Bartůněk, V. Simple synthesis of free surface nanostructured spinel NiFe_2O_4 with a tunable particle size. *J. Alloys Compd.* **2017**, *723*, 58–63. [[CrossRef](#)]
28. Bartůněk, V.; Huber, S.; Luxa, J.; Sofer, Z.; Kuchař, M.; Dobrovolny, K.; Jankovský, O. Facile synthesis of magnetic Co nanofoam by low-temperature thermal decomposition of Co glycerolate. *IET Micro Nano Lett.* **2017**, *12*, 278–280. [[CrossRef](#)]
29. Tudorache, F.; Popa, P.D.; Dobromir, M.; Iacomi, F. Studies on the structure and gas sensing properties of nickel-cobalt ferrite thin films prepared by spin coating. *Mater. Sci. Eng. B* **2013**, *178*, 1334–1338. [[CrossRef](#)]
30. Hill, A.H.; Harrison, A.; Dickinson, C.; Zhou, W.; Kockelmann, W. Crystallographic and magnetic studies of mesoporous eskolaite, Cr_2O_3 . *Microporous Mesoporous Mater.* **2010**, *130*, 280–286. [[CrossRef](#)]
31. Nica, V.; Daniel, G.; Ursu, C.; Tudorache, F.; Brinza, F.; Pui, A. Synthesis and characterization of Co-substituted ferrite nanocomposites. *IEEE Trans. Magn.* **2013**, *49*, 26–29. [[CrossRef](#)]
32. Wang, Z.W.; Downs, R.T.; Pischedda, V.; Shetty, R.; Saxena, S.K.; Zha, C.S.; Zhao, Y.S.; Schiferl, D.; Waskowska, A. High-pressure X-ray diffraction and Raman spectroscopic studies of the tetragonal spinel CoFe_2O_4 . *Phys. Rev. B* **2003**, *68*, 094101. [[CrossRef](#)]
33. Chandramohan, P.; Srinivasan, M.; Velmurugan, S.; Narasimhan, S. Cation distribution and particle size effect on Raman spectrum of CoFe_2O_4 . *J. Solid State Chem.* **2011**, *184*, 89–96. [[CrossRef](#)]
34. Lazzeri, M.; Thibaudeau, P. Ab initio Raman spectrum of the normal and disordered MgAl_2O_4 spinel. *Phys. Rev. B* **2006**, *74*, 140301. [[CrossRef](#)]
35. Repko, A.; Nižňanský, D.; Poltiová-Vejpravová, J. A study of oleic acid-based hydrothermal preparation of CoFe_2O_4 nanoparticles. *J. Nanopart. Res.* **2011**, *13*, 5021. [[CrossRef](#)]
36. Bozorth, R.M.; Tilden, E.F.; Williams, A.J. Anisotropy and Magnetostriction of Some Ferrites. *Phys. Rev.* **1955**, *99*, 1788–1798. [[CrossRef](#)]

